




## Article

# One-Pot Microwave-Assisted Synthesis of Water-Soluble Pyran-2,4,5-triol Glucose Amine Schiff Base Derivative: XRD/HSA Interactions, Crystal Structure, Spectral, Thermal and a DFT/TD-DFT

Yousef Hijji <sup>1,\*</sup> , Rajeesh Rajan <sup>1</sup> , Hamdi Ben Yahia <sup>2</sup>, Said Mansour <sup>2</sup>, Abdelkader Zarrouk <sup>3</sup>  and Ismail Warad <sup>1,\*</sup>

<sup>1</sup> Department of Chemistry and Earth Sciences, Qatar University, Doha 2713, Qatar; rajeesh.Rajan@qu.edu.qa

<sup>2</sup> Qatar Environment and Energy Research Institute, Hamad Bin Khalifa University, Qatar Foundation, Doha 34110, Qatar; benyahiahamdi77@gmail.com (H.B.Y.); smansour@hbku.edu.qa (S.M.)

<sup>3</sup> Laboratory of Materials, Nanotechnology and Environment, Faculty of Sciences, Mohammed V University, 4 Av. Ibn Battuta, Rabat B.P. 1014, Morocco; azarrouk@gmail.com

\* Correspondence: yousef.hijji@qu.edu.qa (Y.H.); ismail.warad@qu.edu.qa (I.W.)

**Abstract:** The (3R,4R,6R)-3-((E)-2-hydroxybenzylidene)amino)-6-(hydroxymethyl)tetrahydro-2H-pyran-2,4,5-triol water-soluble Glucose amine Schiff base (GASB-1) product was made available by condensation of 2-hydroxybenzaldehyde with (3R,6R)-3-amino-6-(hydroxymethyl)-tetra-hydro-2H-pyran-2,4,5-triol under mono-mode microwave heating. A one-pot 5-minute microwave-assisted reaction was required to complete the condensation reaction with 90% yield and without having byproducts. The 3D structure of GASB-1 was solved from single crystal X-ray diffraction data and computed by DFT/6-311G(d,p). The Hirshfeld surface analysis (HSA), molecular electronic potential (MEP), Mulliken atomic charge (MAC), and natural population analysis (NPA) were performed. The IR and UV-Vis spectra were matched to their density functional theory (DFT) relatives and the thermal behavior was resolved in an open-room condition via thermogravimetry/Derivative thermogravimetry (TG/DTG) and differential scanning calorimetry (DSC). The highest occupied molecular orbital/lowest unoccupied molecular orbital (HOMO/LUMO), density of state (DOS), and time-dependence TD-DFT computations were correlated to the experimental electron transfer in water and acrylonitrile solvents.

**Keywords:** crystal structure; Schiff base; DFT; glucose amine; salicylaldehyde



**Citation:** Hijji, Y.; Rajan, R.; Ben Yahia, H.; Mansour, S.; Zarrouk, A.; Warad, I. One-Pot Microwave-Assisted Synthesis of Water-Soluble Pyran-2,4,5-triol Glucose Amine Schiff Base Derivative: XRD/HSA Interactions, Crystal Structure, Spectral, Thermal and a DFT/TD-DFT. *Crystals* **2021**, *11*, 117. <https://doi.org/10.3390/cryst11020117>

Academic Editor:

Alexander S. Novikov

Received: 11 January 2021

Accepted: 22 January 2021

Published: 26 January 2021

**Publisher's Note:** MDPI stays neutral with regard to jurisdictional claims in published maps and institutional affiliations.



**Copyright:** © 2021 by the authors. Licensee MDPI, Basel, Switzerland. This article is an open access article distributed under the terms and conditions of the Creative Commons Attribution (CC BY) license (<https://creativecommons.org/licenses/by/4.0/>).

## 1. Introduction

Glucose amine Schiff bases (GASBs) are common chiral organic compounds that were synthesized decades ago [1–5]. GASBs are an important class of artificial compounds since they have several applications in many life fields [6]. For example, such Schiff bases from food derivatives are used in antibacterial, antimicrobial, antiviral, and other biological activities [7]. Moreover, they have been used in tumor cell imaging, conductive polymers, and optical sensors, as well as for detection of amino acids, fluoride, iron, and other heavy metals [8–10].

In terms of complexes, the greatest benefits of GASBs as ligands are their solubility in water and multidentate coordination possibilities. Moreover, the ring conformations or configurations of the pyran ring in glucose center increase the chance of bonding in different coordination modes. The complexes of such GASBs with metal ions have several applications as catalysts, for example, in oxygenations, hydrolysis, and anticorrosion [11–15]. The presence of several chiral centers loaded in GASBs backbone increases the possibility of using their complexes to prepare chiral catalysts or chiral reagents. For example, vanadium oxides/GASB was used in chiral oxidation of sulfides [16].

Recently, microwave technology has been used in Schiff base preparation instead of traditional methods, as this technology has achieved global acceptance in accelerating the reaction and increasing its selectivity, which has reduced the formation of side products. Moreover, the displayed reactions without or with a minimum number of solvents has increased the chance of imposing green chemistry technology [17–19].

In this work, we report efficient ecofriendly microwave synthesis under mild condition of a water-soluble sugar derivative GASB-1 within 5 min at 60 °C under microwave heating conditions. The pyran chair conformation structure was confirmed by single-crystal X-ray diffraction (XRD) where no ring opening was detected. Furthermore, the XRD/Hirshfeld surface analysis (HSA) interactions and XRD/DFT analyses were performed, and the physicochemical properties, such as IR and UV-visible, were matched to B3LYP and TD-DFT, respectively. The thermal properties were also evaluated through TG/DTG and DSC.

## 2. Experimental

### 2.1. Measurements

The Fourier transform infrared spectrum (FT-IR) (MID. 4000–400  $\text{cm}^{-1}$ ) was recorded in solid state using a PerkinElmer Spectrum 1000 FT-IR Spectrometer (PerkinElmer Inc., Waltham, MA, USA). The UV-Vis measurements were performed in water solvent using a TU-1901 double-beam spectrophotometer (Purkinje General Instrument Co., Ltd., Beijing, China). The TG spectra were recorded using a TGA-7 PerkinElmer (PerkinElmer Inc., Waltham, MA, USA) in 25 to 600 °C temperature range and with heat rate = 5 °C  $\text{min}^{-1}$ . The microwave reactions were carried out with a Biotage initiator 8 instrument (Biotage, Uppsala, Sweden).

### 2.2. Computational

The crystallographic CIF file generated from single-crystal XRD was taken as reference for HSA calculations using the CRYSTAL EXPLORER software (version 17, University of Western Australia, Perth, Australia) [20]. All the DFT calculations were carried out using gaussian (revision 09, Gaussian Inc., Wallingford, CT, USA) software and considering a gaseous state at DFT/B3LYP/6-311G(d,p) [21]. The DFT data were visualized using GaussSum (Version3.9, Gaussian Inc., Wallingford, CT, USA) [22] and Gaussview software (version 05; Semichem Inc., Shawnee, OK, USA) [23].

### 2.3. Crystal Data

Suitable single crystals for X-ray diffraction were selected based on the size and sharpness of the diffraction spots. The data collections were carried out on a D8 Venture diffractometer using Cu-K $\alpha$  radiation (Bruker GmbH, Berlin, Germany). Data processing and all refinements were performed with the APEX3 and Jana2006 program package, respectively [24,25]. Multiscan absorption corrections using SADABS were applied for data collection details, as shown in Table 1.

Table 1. Refined data of the GASB-1 Crystal.

Chemical Formula	$C_{13}H_{17}NO_6$
CCDC	2054297
$M_r$	283.3
Flack parameter	0.4(9)
Crystal system, space group	Monoclinic, C2
Temperature (K)	150
$a, b, c$ (Å)	18.438 (3), 6.0431 (11), 13.133 (2)
$\beta$ (°)	117.486 (7)
$V$ (Å <sup>3</sup> )	1298.1 (4)
$Z$	4
Radiation type	Cu $K\alpha$
$\mu$ (mm <sup>-1</sup> )	0.98
Crystal size (mm)	0.26 × 0.06 × 0.03
	Data collection
Diffractometer	Bruker D8 VENTURE
Absorption correction	Multi-scan SADABS
$T_{min}, T_{max}$	0.884, 1
No. of measured, independent and observed [ $I > 4\sigma(I)$ ] reflections	4820, 1667, 674
$R_{int}$	0.104
$(\sin \theta / \lambda)_{max}$ (Å <sup>-1</sup> )	0.597
	Refinement
$R[F^2 > 2\sigma(F^2)], wR(F^2), S$	0.068, 0.228, 1.01
No. of reflections	1667
No. of parameters	196
No. of restraints	10
$\Delta\rho_{max}, \Delta\rho_{min}$ (e Å <sup>-3</sup> )	0.39, -0.25
Absolute structure	486 of Friedel pairs used in the refinement

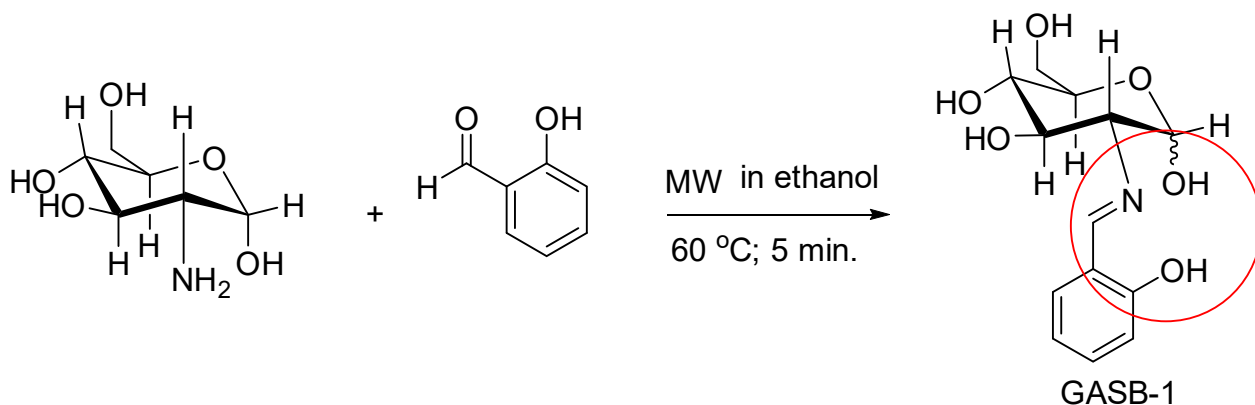
#### 2.4. GASB-1 Synthesis

Glucosamine hydrochloride (0.884 gm, 1 mmol) was treated in 4 mL ethanol with triethylamine. To the mixture, salicylaldehyde (0.432 mL, 1.1 mmol) was added in a microwave vial. The vial was capped and heated in the microwave synthesizer at 60 °C for 5 min, which led immediately to the formation of a bright yellow precipitate. The vial was then cooled to room temperature. The yellow solid was filtered and washed with cold ethanol then recrystallized from ethanol to afford the desired GASB-1 (90%) as bright-yellow crystals. Recrystallization from ethanol again provided very nice yellow crystals which were used for X-ray diffraction.

### 3. Results and Discussion

#### 3.1. Microwave Synthesis

The use of microwave-assisted techniques in the preparation of Schiff bases is of high interest in the organic green synthesis field. The condensation of (3R,6R)-3-amino-6-(hydroxymethyl)-tetrahydro-2H-pyran-2,4,5-triol with 2-hydroxybenzaldehyde under nonroutine microwaved condition using ethanol solvent revealed the formation of the desired GASB-1 in 90% yield, as illustrated in Scheme 1. A 5-minute reaction is required to synthesize the desired ligand without byproducts. Moreover, microwave-assisted techniques involve simple handling, making them a cheaper and quicker synthetic method than the classical methods reported [16–19].



**Scheme 1.** Synthesis of desired compound GASB-1.

### 3.2. XRD and DFT

The desired ligand was subjected to XRD and DFT calculation, and the Oak Ridge Thermal Ellipsoid Plot (ORTEP) and B3LYP/6-311G(d,p)-optimized diagram are illustrated in Figure 1a,b, respectively. The DFT/XRD angles and bond lengths are illustrated in Table 2. A packing diagram, viewed down the *b* axis, is given in Figure 1c. The desired compound was crystallized in a monoclinic, *C*2 space group (*Z* = 4). The stair-like structure is two-dimensional. In the flat aromatic ring C8-C9-C0-C11-C12-C13, all the carbon atoms have an  $sp^2$  hybridization, whereas in the pyranose ring O1-C1-C2-C3-C4-O5, which has a chair conformation [26] with the puckering parameters  $Q = 0.584(9)$  Å,  $\theta = 2.6(9)^\circ$  and  $\varphi = 65(16)^\circ$  [27], all the atoms have an  $sp^3$  hybridization.

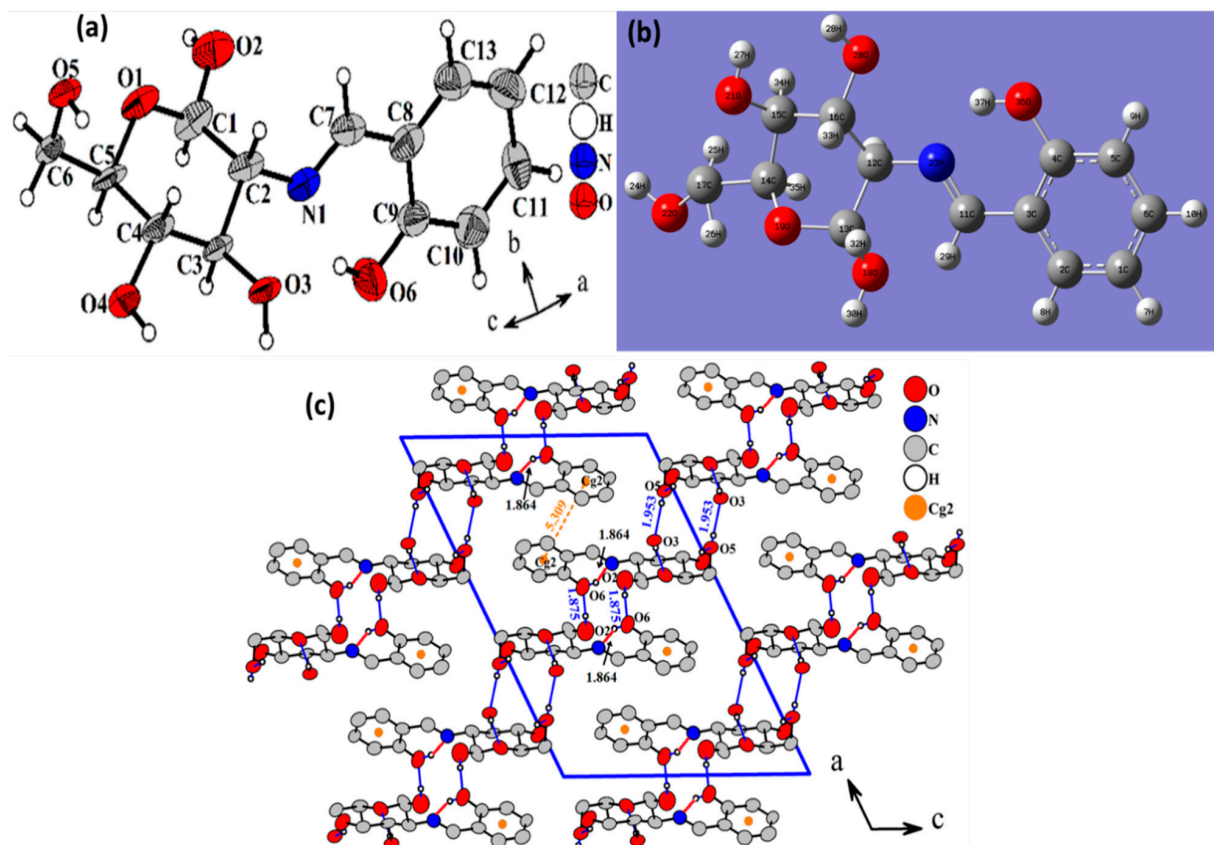


**Figure 1.** (a) ORTEP, (b) B3LYP/6-311G(d,p), and (c) packing diagrams viewed down the *b* axis.

**Table 2.** Elected X-ray diffraction (XRD)/DFT angles ( $^{\circ}$ ) and bond lengths ( $\text{\AA}$ ).

No.	Bond		XRD	DFT	No.	Angle			XRD	DFT
1	O1	C1	1.41(1)	1.417	18	C1	O1	C5	113.9(6)	112.5
2	O1	C5	1.44(1)	1.434	19	C2	N1	C7	120.6(7)	121.83
3	O2	C1	1.28(1)	1.302	20	O1	C1	O2	108.6(7)	109.08
4	O3	C3	1.419(9)	1.422	21	O1	C1	C2	107.9(7)	108.67
5	O4	C4	1.41(1)	1.405	22	O2	C1	C2	113.9(8)	113.68
6	O5	C6	1.413(8)	1.405	23	N1	C2	C1	109.9(7)	108.38
7	O6	C9	1.32(1)	1.342	24	N1	C2	C3	111.2(7)	112.94
8	N1	C2	1.48(1)	1.502	25	C1	C2	C3	109.6(7)	108.38
9	N1	C7	1.27(1)	1.254	26	O3	C3	C2	110.3(6)	109.5
10	C1	C2	1.55(1)	1.561	27	O3	C3	C4	111.0(6)	111.85
11	C2	C3	1.52(1)	1.521	28	C2	C3	C4	109.6(7)	110.83
12	C3	C4	1.50(1)	1.498	29	O4	C4	C3	113.5(7)	113.68
13	C4	C5	1.53(1)	1.515	30	O4	C4	C5	105.3(6)	107.61
14	C5	C6	1.51(1)	1.521	31	C3	C4	C5	111.2(6)	113.68
15	C7	C8	1.48(1)	1.476	32	O1	C5	C4	109.2(6)	111.33
16	C8	C9	1.39(1)	1.372	33	O1	C5	C6	107.1(6)	109.26
17	C8	C13	1.36(2)	1.367	34	C4	C5	C6	114.3(6)	111.96

The experimental XRD angles and bond distances were emulated to the DFT/B3LYP/6-311++G(d,p) as showed in Figure 2. The bonds lengths reflected a high proper between calculated and measured (Figure 2a) with 0.977 correlation coefficient as seen in Figure 2b. The DFT/XRD angles values reflected a high degree of similarity (Figure 2c) with a 0.941 correlation coefficient as seen Figure 2d.

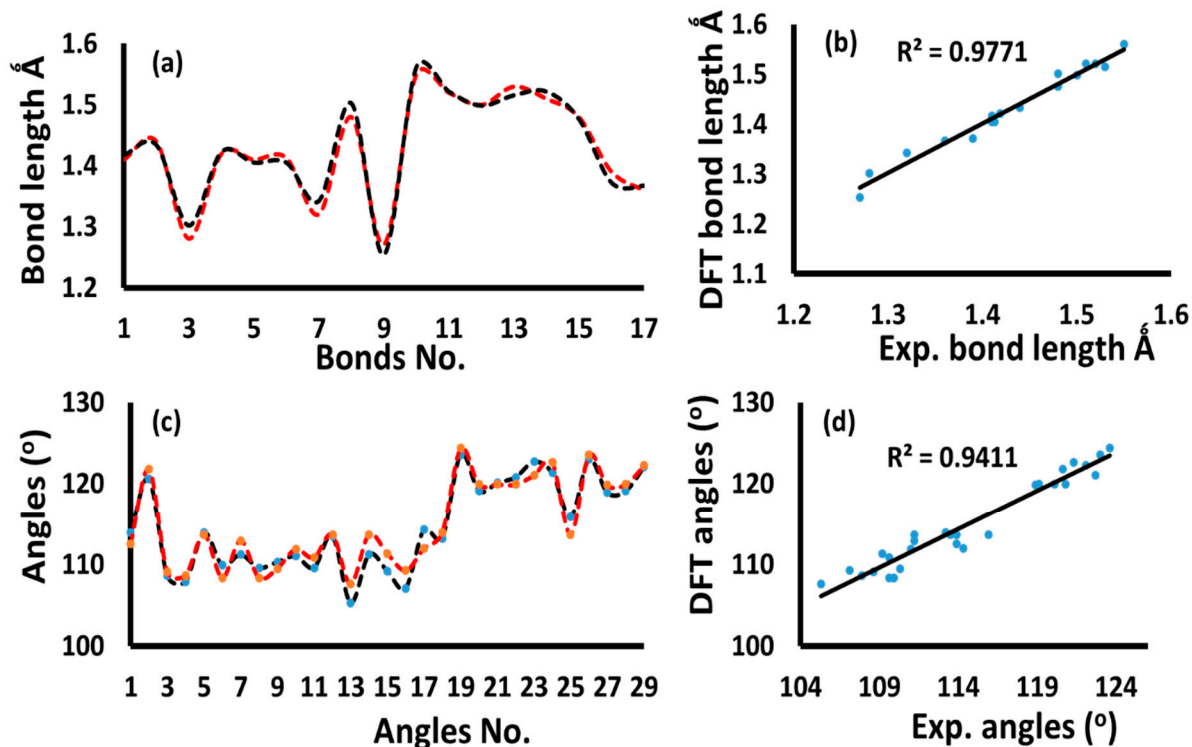


**Figure 2.** (a) DFT/XRD bond length histogram and its (b) graphical correlation, (c) DFT/XRD angles histogram, and (d) graphical correlation.



### 3.3. XRD Packing and HSA

In the XRD packing result, several short interactions stabilized the crystal lattice of the desired Schiff base, as seen in Table 3 and Figure 3. The first interaction was detected as an intra-hydrogen bond, such as O-H ... N=C, with 1.864 Å forming a close S6 as seen in Figure 3a. The second type of interaction was 1D hydrogen bond, such as Ph-H ... O-C with 2.580 Å, resulting a continuous chain as seen in Figure 3b. The third type was 2D-S6-synthon with two hydrogen bonds, such as O-H ... O, with 1.953 Å and Ph-H ... O with 2.563 Å, as seen in Figure 3c. The fourth type was a 2D-S4 synthon with three hydrogen bonds of type O-H ... O with 2.089 Å, 2.568 Å, and 2.005 Å, as seen in Figure 3d. The fifth interaction was H ...  $\pi_{C9-C8}$  type with 2.840 Å as seen in Figure 3e.

**Table 3.** All hydrogen bond types.

Donor	Hydrogen	Acceptor	D-H Distance	H...A Distance	D-A Distance	D-H...A Angle
O2	H1O2	O6	0.83(6)	1.87(7)	2.684(10)	168(8)
O3	H1O3	O1	0.821(16)	2.09(3)	2.885(7)	164(5)
O4	H1O4	O5	0.82(6)	2.01(5)	2.727(7)	146(9)
O5	H1O5	O3	0.819(19)	1.95(2)	2.725(6)	157.2(16)
O6	H1O6	N1	0.82(6)	1.86(6)	2.596(9)	148(9)

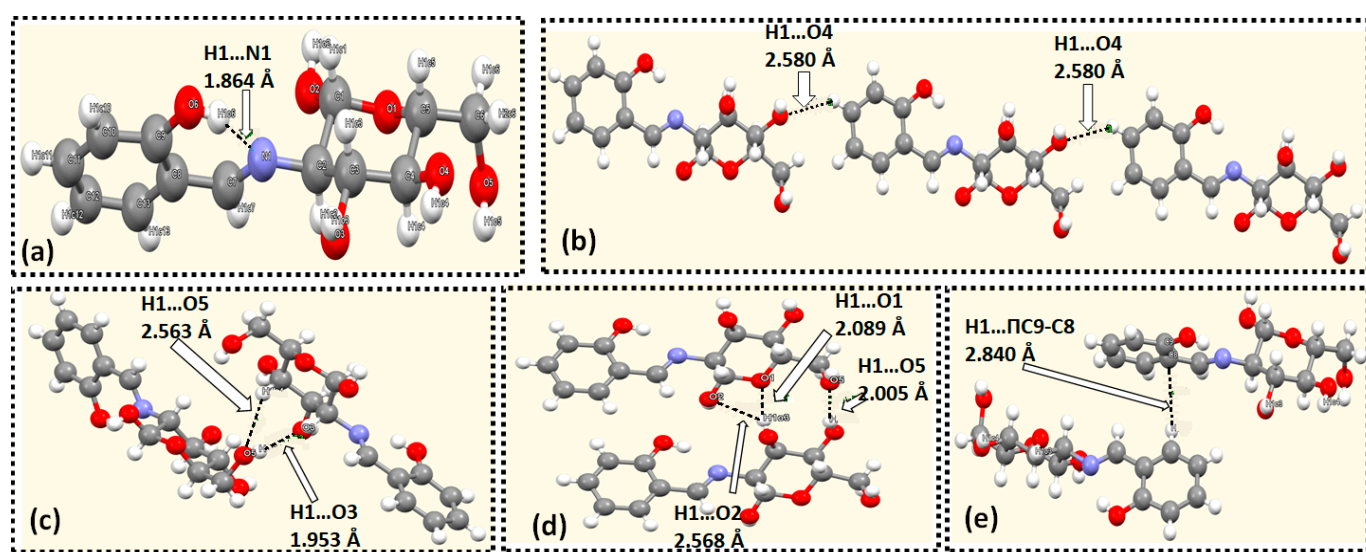


**Figure 3.** (a) OH ... N intraH-bond, (b) Ph-H ... O interH-bond, (c) 2D-S6-synthon, (d) 2D-S4 synthon, and (e) H ...  $\pi_{C9-C8}$  interactions types in the GASB-1 lattice.

The HSA calculation of the prepared Schiff base was carried using the CIF file generated from single crystal XRD. The interactions were shown as a red point on the GASB-1 surface [28–35]. The desired Schiff base contains many OH and O atoms in the sugar part together with N=C in the Schiff base part. Therefore, nine red spots were detected by  $d_{norm}$  on the surface, reflecting the presence of different types of [OH ... O] hydrogen bonds connected the computed surface of the molecule with its surrounding neighboring molecules. Moreover, a big red spot occurred around the N atom due to the [O-H ... N] intra-hydrogen bond (Figure 4a). The presence of only one type of H ...  $\pi_{C=C}$  interaction was confirmed by the shape index as seen in Figure 4b. Moreover, the fingerprint (FP) H-to-atom connection ratio plot reflected the diversity of the percentage contribution. The highest interaction ration was H...H bonds contribution with 45.5%, while the lowest interaction ration was N...H contribution with 0.5%. The

FP result revealed all the H-connections percentage contributions in the following order: [H...H>O...H(14.6%)>C...H(8.9%)>N...H(0.5%)].

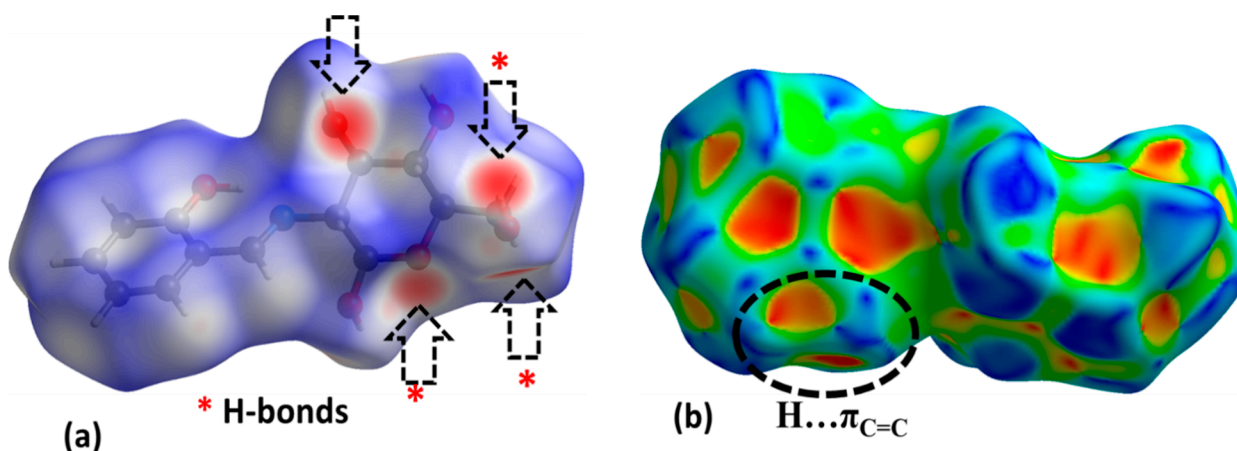


Figure 4. (a)  $d_{norm}$ , (b) shape index.

#### 3.4. Molecular Electrostatic Potential (MEP), Mulliken Atomic Charge (MAC), and Natural Population Analysis (NPA)

On the surface of the desired molecule, the MEP calculation revealed the presence of red (nucleophilic), blue (electrophilic), and green (not polarized) positions [26–30]. All the O and N atoms and some C atoms were nucleophilic in their nature. Moreover, all the H atoms attached to O atoms were blue in color, resulting in electrophilic centers (Figure 5a). The other centers in the compounds were green since they were in between electrophilic and nucleophilic centers. The presence of H<sub>2</sub> acceptors together with electron donor centers, encourage the formation of intra-[H...N] and inter-[H...O] hydrogen bonds.

The NPA and MAC supported the MEP result in founding both e-rich/poor atoms sites on the molecule. The NPA- and MAC-computed charges revealed all the atoms with a negative or positive quantity of charge as represented in Figure 5b and Table 4. Usually, the NPA displayed higher atomic charges compared to the MAC. As expected, the MAC and NPA evidenced all O, N, C1-C6, and C13 atoms with negative charges and all the H, C14-C17, and C12 atoms are with positive charges. H31 is among the highest atoms with a positive charge. Therefore, it is responsible for forming the intra-H-bond of type O-H...N bond. The NPA and MAC charge model reflected a high degree of matching, and  $R^2 = 0.9462$  was detected, as shown in Figure 5c. The MAC, NPA, and MEP data are highly harmonic with HSA and XRD results.

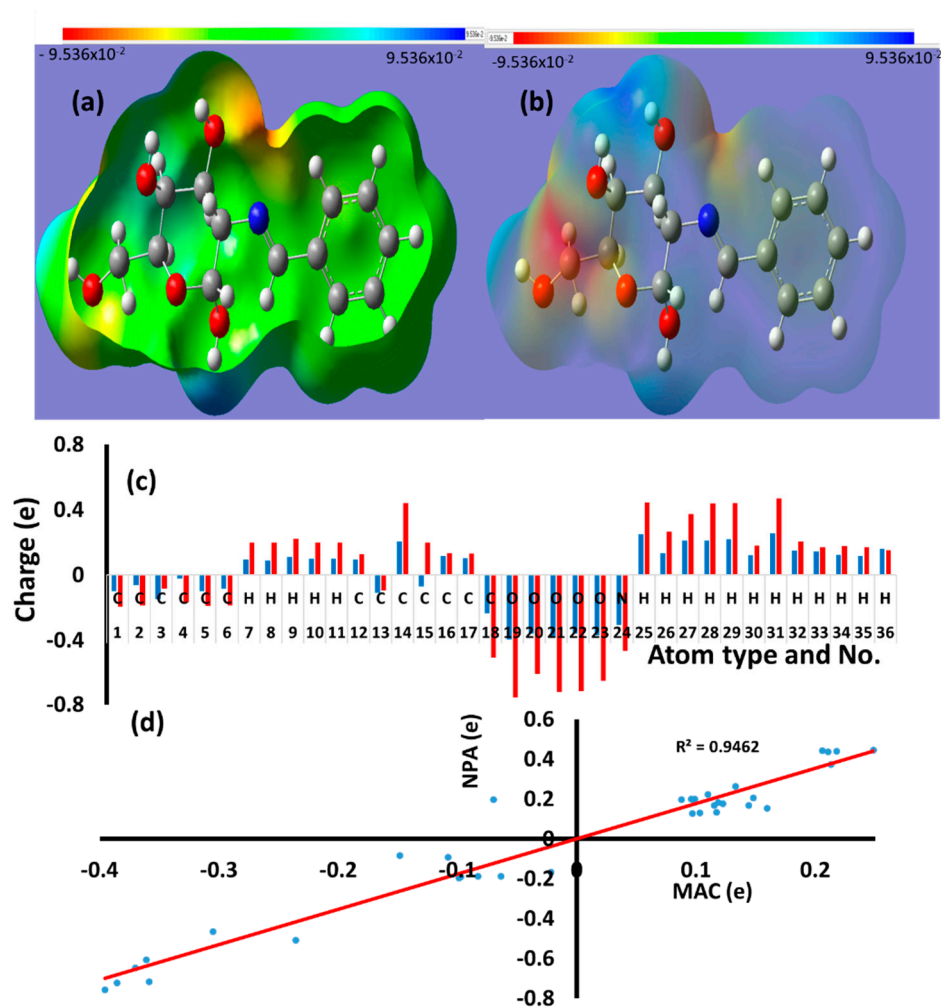


Figure 5. (a) Solid MEP, (b) open MEP, (c) MAC and NPA charges and (d) MAC vs. NPA relation.

Table 4. NPA and MAC charges.

No.	Atom	MAC	NBA	No.	Atom	MAC	NBA
1	C	-0.0986	-0.19484	19	O	-0.39559	-0.75684
2	C	-0.06331	-0.18638	20	O	-0.36058	-0.60764
3	C	-0.14837	-0.0848	21	O	-0.38535	-0.72255
4	C	-0.02168	-0.1673	22	O	-0.35858	-0.71719
5	C	-0.09702	-0.1905	23	O	-0.36984	-0.6475
6	C	-0.08268	-0.18756	24	N	-0.30484	-0.46408
7	H	0.095839	0.19838	25	H	0.249019	0.44549
8	H	0.087757	0.19803	26	H	0.13298	0.26307
9	H	0.109898	0.2228	27	H	0.213206	0.37366
10	H	0.099062	0.19882	28	H	0.210967	0.43698
11	H	0.097445	0.19754	29	H	0.217824	0.44051
12	C	0.097101	0.12806	30	H	0.118774	0.18125
13	C	-0.10795	-0.09328	31	H	0.253056	0.4681
14	C	0.205948	0.4415	32	H	0.148058	0.20596
15	C	-0.06965	0.19739	33	H	0.144472	0.16871
16	C	0.117445	0.13276	34	H	0.122554	0.17625
17	C	0.103363	0.12963	35	H	0.115282	0.16932
18	C	-0.2357	-0.50734	36	H	0.159658	0.1536



### 3.5. IR, B3LYP, and NMR Investigation

In the IR spectrum shown in Figure 6a, the stretching vibration bands at  $3405\text{ cm}^{-1}$ ,  $3070\text{ cm}^{-1}$ ,  $2960\text{--}2860\text{ cm}^{-1}$ ,  $1630\text{ cm}^{-1}$ ,  $1200\text{--}1000\text{ cm}^{-1}$ , and  $1100\text{--}900\text{ cm}^{-1}$  are characteristic of the functional groups O-H,  $\text{C}_{\text{ph}}\text{-H}$ ,  $\text{C}_{\text{Me}}\text{-H}$ , C=N, C=C, C-O, and C-N, respectively. Furthermore, the DFT-IR/B3LYP/6-311G(d,p) in gaseous state supported the experimental IR analysis with the presence of O-H at  $3480\text{ cm}^{-1}$ ,  $\text{C}_{\text{ph}}\text{-H}$  at  $3120\text{ cm}^{-1}$ ,  $\text{C}_{\text{Me}}\text{-H}$  at  $2980\text{--}2880\text{ cm}^{-1}$ , C=N at  $1610\text{ cm}^{-1}$ , C=C at  $1230\text{ cm}^{-1}$ , C-O at  $1280\text{--}1090\text{ cm}^{-1}$ , and C-N at  $750\text{--}840\text{ cm}^{-1}$ , as shown in Figure 6b. The experimental/DFT-IR showed a high affinity with a high coefficient ( $R^2 = 0.998$ ) as recorded in Figure 6c.

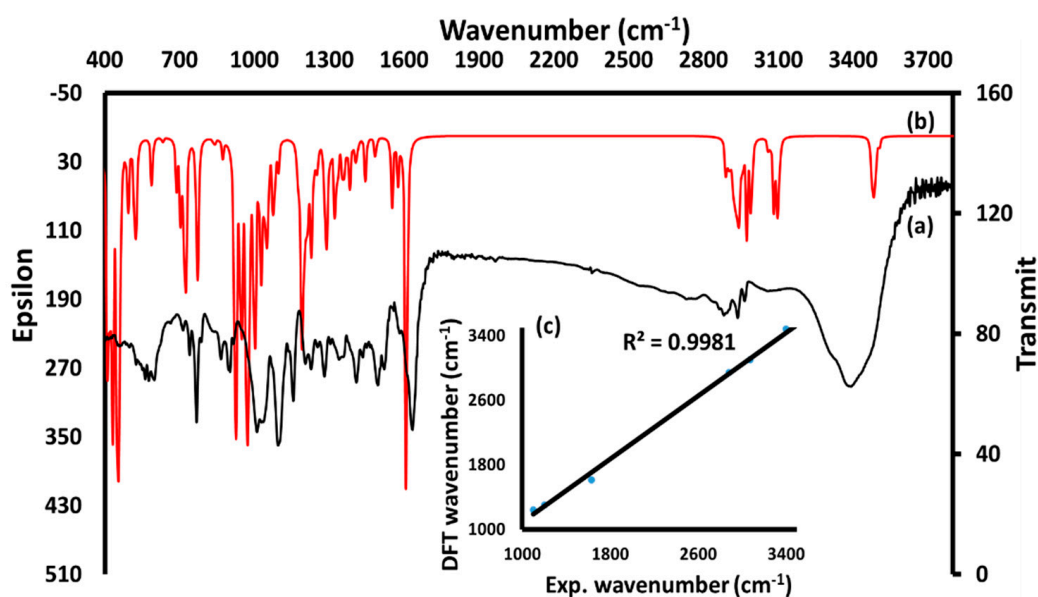


**Figure 6.** (a) Experimental solid-state IR, (b) Gaseous-state DFT-IR, and (c) Experimental DFT-IR correlation.

The structure of GASB-1 was elucidated and confirmed by the data obtained from the  $^1\text{H}$  NMR and  $^{13}\text{C}$ -NMR spectra in DMSO-*d*<sub>6</sub> presented in Figure 7a and Figure 7b, respectively. In the  $^1\text{H}$ NMR, the spectra displayed several bands. The sugar protons were recorded at 2.5–5.5 ppm, the aromatic protons at 6.5–7.5 ppm, and the acidic phenolic proton and imine proton appeared at 13.20 ppm 8.25 ppm, respectively. In  $^{13}\text{C}$ -NMR, the sugar carbons were detected in between 60–100 ppm, the aromatic carbons in between 115–135 ppm, and the imine and phenolic carbon signals appeared at 167.21 ppm and 160.99 ppm, respectively (see the experimental part). The protons and carbons NMR chemical shifts are consistent with the proposed structure solved by single-crystal XRD.

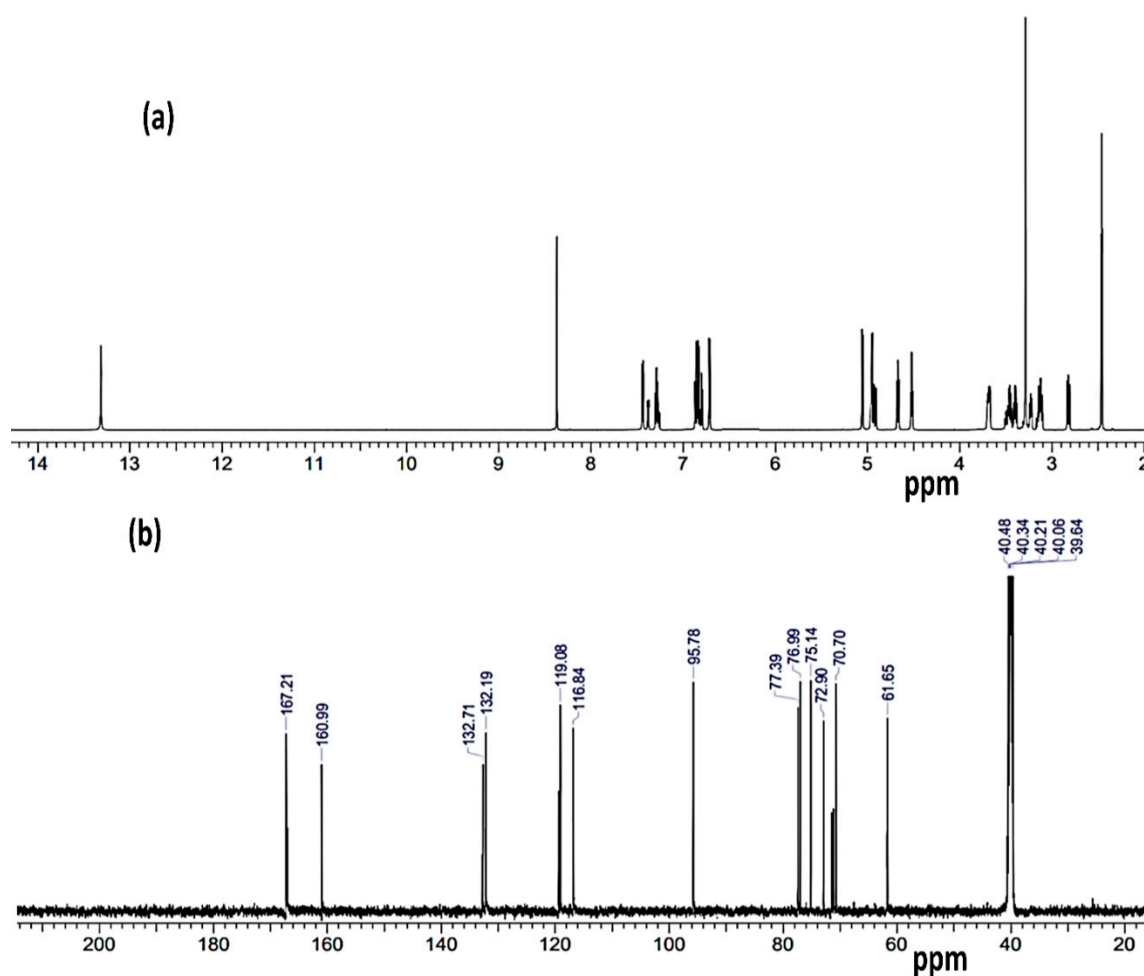


Figure 7. (a)  $^1\text{H}$ , (b)  $^{13}\text{C}$ -NMR of GASB-1 dissolved in DMSO- $d_6$ .

### 3.6. HOMO/LUMO and Absorption/TD-DFT

The HOMO $\rightarrow$ LUMO orbital shapes (Figure 8a) and energy diagrams were performed using GaussView 5.0 software. The LUMO and HOMO molecular orbital energy levels both had negative values. Thus, the stability and softness of the GASB-1 were increased. The  $\Delta E_{\text{HOMO/LUMO}}$  was found to be 1.730 eV, whereas the  $\Delta E_{\text{DOS}}$  was 1.784 eV. A negligible deviation between the two methods was detected.

The UV-visible for the desired sugar derivative Schiff base was measured in water and acetonitrile solvents in the scale of 200–800 nm, parallel to that ground-state TD-DFT/B3LYP/6-31G(d,p) scale of theory computation. The measurement was performed to collect the oscillator strength ( $f$ ), vertical excitation energies and absorption wavelength (nm) as seen in Table 5. The  $\lambda_{\text{max}}$  in the spectrum reconciled to vertical excitation as per the Frank–Condon principle. Both of theoretical and experimental spectra are plotted in Figure 8b. The experimental UV-visible in water indicated the presence of four peaks. The first three bands at  $\lambda_{\text{max}} = 215$  nm, 255 nm, and 328 nm are attributed to  $\pi\rightarrow\pi^*$ ,  $\pi\rightarrow n$ , and  $n\rightarrow\pi^*$  electron transfer in the desired Schiff base, respectively. Meanwhile, the fourth peak, which was detected at  $\lambda_{\text{max}} = 395$  nm, can be attributed to the dissociation of the phenol to form the phenolate ion in aqueous polar medium as indicated in Scheme 2. The absence of this band in nonpolar solvent as  $\text{CH}_3\text{CN}$  confirmed this aspect (Figure 8b).

Table 5. TD-DFT data for GASB-1 in water.

No.	$\lambda$ (nm)	Osc. Str. (f)	Major Contribution	Minor Contribution
1	545.9	0.0116	HOMO->L+1(100%)	
2	317.1	0.0015	H-2->LUMO(76%), H-1->LUMO(18%)	H-4->LUMO(2%)
3	309.1	0.0205	H-2->LUMO(20%), H-1->LUMO(73%)	H-4->LUMO(5%)
4	307.3	0.0165	H-6->LUMO(13%), H-5->LUMO(18%), H-4->LUMO(57%)	H-7->LUMO(3%), H-1->LUMO(6%)
5	294.2	0.0028	H-2->L+1(93%)	H-2->L+3(2%), H-1->L+1(3%)
6	276.9	0.0073	H-6->LUMO(73%), H-5->LUMO(20%)	H-7->LUMO(4%)
7	270.1	0.0035	HOMO->L+3(86%), HOMO->L+4(14%)	
8	267.6	0.0303	HOMO->L+3(13%), HOMO->L+4(84%)	
9	255.8	0.0121	H-3->L+1(78%), H-1->L+2 (19%)	H-1->L+1 (3%)
10	247.5	0.5811	H-1->L+1(97%)	H-2->L+1 (3%)
11	241.1	0.0104	H-7->LUMO(86%)	H-9->LUMO(3%), H-5->LUMO(9%)
12	230.9	0.0007	H-4->L+1(95%)	HOMO->L+6(2%)
13	230.1	0.0062	HOMO->L+6(94%)	H-4->L+1(2%)
14	224.9	0.0126	H-9->LUMO(14%), H-8->LUMO(76%)	HOMO->L+5(8%)
15	223.4	0.0047	HOMO->L+5 (91%)	H-9->LUMO(3%), H-8->LUMO(5%)
16	218.7	0.0380	H-9->LUMO(67%), H-8->LUMO(16%)	H-10->LUMO(9%), H-7->LUMO(3%)
17	215	0.0027	H-5->L+1(88%)	H-6->L+1(8%)
18	207.3	0.0064	HOMO->L+7(14%), HOMO->L+8(15%), HOMO->L+9(68%)	
19	204.8	0.0217	HOMO->L+7(12%), HOMO->L+8(52%), HOMO->L+9(26%)	H-1->L+2(4%)

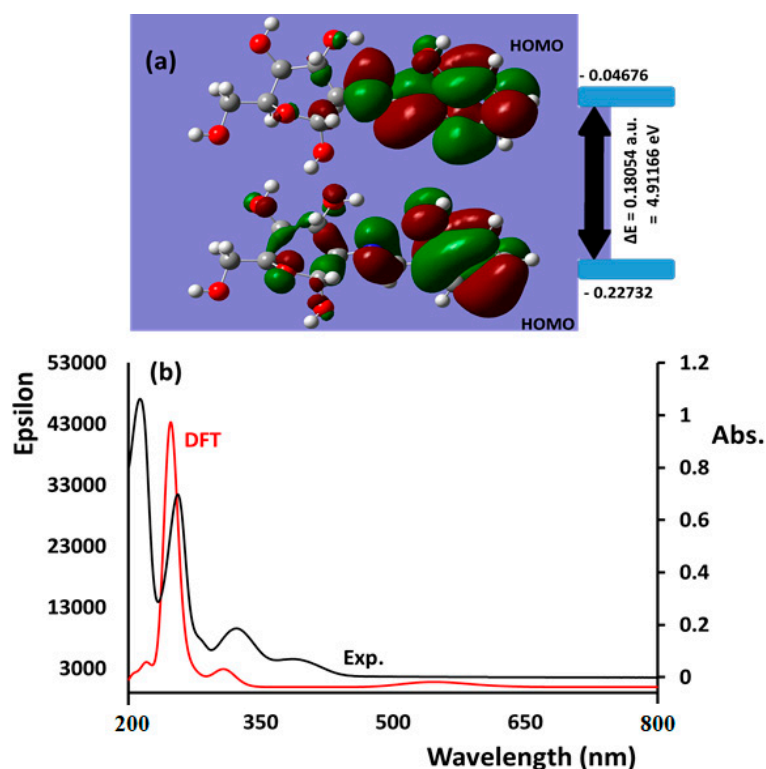
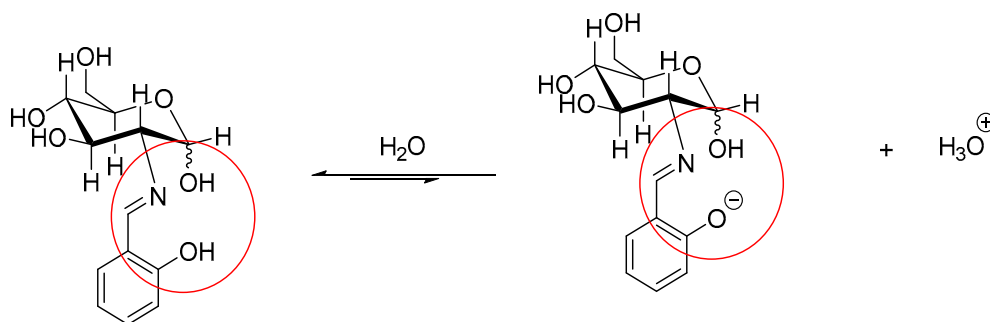


Figure 8. (a) LUMO/HOMO, and (b) Abs./TD-DFT spectra in water and acetonitrile.



**Scheme 2.** Dissociation of the phenolic Schiff base in water polar medium.

The DFT calculations for B3LYP/6-31G(d,p) in the same solvents demonstrated the presence of three main bands at  $\lambda_{\max} = 247.5$  nm, 309.1 nm, and 545.9 nm, with oscillator strengths of 0.5811, 0.0205, and 0.0116, respectively. The band at 247.5 nm can be attributed to the contributions of HOMO-1  $\rightarrow$  LUMO+1 (97%) and HOMO-2  $\rightarrow$  LUMO+1 (3%). The second band at 309.1 nm was due to HOMO-2  $\rightarrow$  LUMO (20%), HOMO-1  $\rightarrow$  LUMO (73%), HOMO-4  $\rightarrow$  LUMO (5%), and the third band at 545.9 nm was due to HOMO  $\rightarrow$  LUMO+1 (100%) electron transfers. In the TD-DFT of the GASB-1, the protic (water) and aprotic (acetonitrile) solvents showed similar behavior. Moreover, a good agreement between the experimental and the theoretical solvato-behavior using protic and aprotic solvents was recorded.

### 3.7. Thermal Analysis

TG/DTG and DSC thermal analyses of the desired GASB were performed in the temperature ranges of 25 °C to 500 °C and 25 °C to 300 °C with the heating rate of 5 °C min<sup>-1</sup>, respectively. The results are illustrated in Figure 9a,b, respectively. GASB-1 decomposed in a one-step process in between 200–300 °C and showed a high stability up to ~200 °C. With TDTG = 196 °C, 100% of mass loss (complete decomposition) was recorded as seen Figure 9a. The DSC was consistent with the TG/DTG. During the heating process from 25 °C to 300 °C, the first peak was due to recrystallization at  $T = 188$  °C followed by a decomposition peak at  $T = 196$  °C. In the reversed cooling process, no peaks were detected (Figure 9b). This confirms the total decomposition of the compound during the heating process.

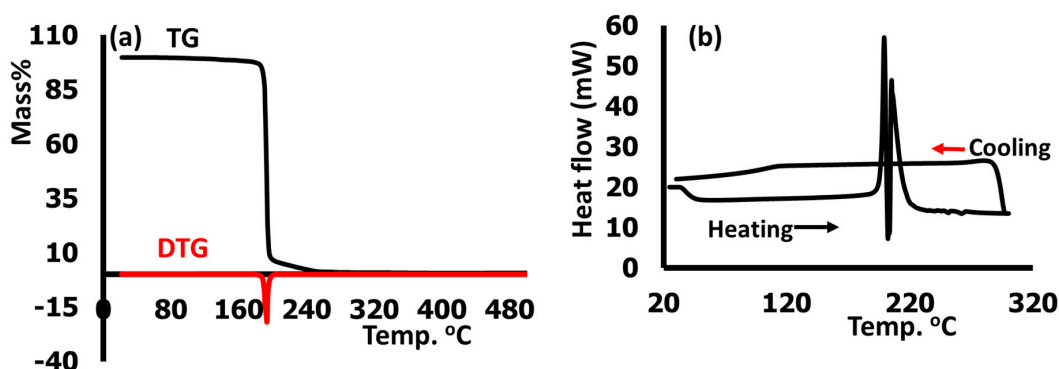


**Figure 9.** (a) TG/DTG and (b) DSC diagrams.

## 4. Conclusions

The desired water-soluble GASB-1 was made available via the one-pot microwave-assisted synthesis method, and its monoclinic structure (space group C2) was confirmed by single-crystal XRD analysis for the first time. The XRD/HSA-interactions was corroborated

by MEP, MAC, and NPA analyses. Several types of short interactions, such as intra-[H . . . N] and inter-[H . . . O] hydrogen bonds in addition to H . . .  $\pi_{C=C}$ , were observed. The calculated DFT angles and bond distances revealed a high matching with the experimental XRD data. The HOMO/LUMO and DOS, together with the computed TD-SCF B3LYP/6-311G(d,p) in water and acetonitrile, reflected an excellent agreement with experimental UV-Visible in the same solvents. The GASB was found to be stable below 196 °C and went through a simple one-step decomposition mechanism.

**Author Contributions:** Y.H.; Conceptualization, methodology, investigation and editing, R.R.; investigation and formal analysis, H.B.Y.; investigation and visualization, S.M.; investigation, A.Z.; software, I.W.; investigation and writing—original draft. All authors have read and agreed to the published version of the manuscript.

**Funding:** This work was made possible by NPRP grant # 7-495-1-094 from Qatar National Research Fund (a member of Qatar Foundation). The findings achieved herein are solely the responsibility of the authors. The authors acknowledge the support by Qatar University through grant # QUCG-CAS-20/21-1.

**Acknowledgments:** The authors acknowledge The Central Laboratory Unit, Qatar University for recording NMR spectra and the contribution of the Core Labs at Qatar Environment and Energy Research Institute (QEERI) at Hamad Bin Khalifa University (HBKU) for the single crystal XRD data analysis.

**Conflicts of Interest:** The authors declare no conflict of interest.

## References

1. Weng, Q.; Yi, J.; Chen, X.; Luo, D.; Wang, Y.; Sun, W.; Kang, J.; Han, Z. Rising from the horizon: Three-dimensional functional architectures assembled with MXene nanosheets. *ACS Omega* **2020**, *5*, 24864. [[CrossRef](#)]
2. Safoura, F. Novel Synthesis of Schiff bases Bearing Glucosamine Moiety. *Res. J. Chem. Sci.* **2014**, *4*, 25.
3. Thanh, D.; van Quoc, N. Study on Synthesis of 2-(Substituted Benzylidene)amino-2-Deoxy-1,3,4,6-Tetra-O-Acetyl- $\beta$ -D-Glucopyranoses from D-Glucosamine. *Lett. Org. Chem.* **2013**, *10*, 85. [[CrossRef](#)]
4. Appelt, R.; Oliveira, S.; Santos. Synthesis and Antimicrobial Activity of Carbohydrate Based Schiff Bases: Importance of Sugar Moiety. *V. Int. J. Carbohydr. Chem.* **2013**, *2013*, 320892. [[CrossRef](#)]
5. Li, Y.; Liu, P. Synthesis of Novel D-glucosamine Schiff Bases. *Chinese J. Synthetic Chem.* **2006**, *14*, 523.
6. Ghoneim, A.; El-Sherif, A. Review on Synthesis of N-glucosylamine Derivatives and Their Biological Activity. *J. Chem. Pharm. Res.* **2019**, *11*, 20.
7. Garoufis, A.; Hadjikakou, K.; Hadjiliadis. Palladium coordination compounds as anti-viral, anti-fungal, anti-microbial and anti-tumor agents. *N. Coordin. Chem. Rev.* **2009**, *253*, 1384. [[CrossRef](#)]
8. Rao, P.; Chinta, P.; Mitra, A. Selective Detection of Aromatic Alpha-Amino Acids and Derivatives Thereof. US20120091355A1, 19 October 2010.
9. Arabahmadi, R. Amani, Azo Schiff bases as colorimetric and fluorescent sensors for recognition of F<sup>-</sup>, Cd<sup>2+</sup> and Hg<sup>2+</sup> ions. *S. Supramol. Chem.* **2014**, *26*, 321. [[CrossRef](#)]
10. Mitra, A.; Ramanujam, B.; Rao, P. 1-(d-Glucopyranosyl-2-deoxy-2-iminomethyl)-2-hydroxynaphthalene as chemo-sensor for Fe<sup>3+</sup> in aqueous HEPES buffer based on colour changes observable with the naked eye. *Tetrahedron Lett.* **2009**, *50*, 776. [[CrossRef](#)]
11. Feng, J.; Le, F.; Luo, H.Q. Synthesis and Characterization of Cobalt(III) Zinc(II) and Copper(II) Complexes with N-Salicylaldehyde-D-Glucosamine and N,O-Vanillin-D-Glucosamine. *Synth. React. Inorg. Met. Org. Chem.* **1998**, *28*, 1105.
12. Ye, Y.; Hu, J.; Feng, C.; Zeng, Y. Synthesis and Reactivity in Inorganic and Metal-Organic Chemistry. *Wuhan Univ. J. Nat. Sci.* **1997**, *2*, 467.
13. Gupta, C.; Sutar, K. Coordin. Coordination chemistry of some new Cu(II), Ni(II) and Co(II) macrocyclic (N<sub>2</sub>O<sub>4</sub>) Schiff base complexes: X-ray crystal structure of Cu(II) complex. *Chem. Rev.* **2008**, *252*, 1420.
14. Bagherzadeh, M.; Amini, M.; Derakhshandeh, G.; Haghdoost. An efficient glucose-based ligand for Heck and Suzuki coupling reactions in aqueous media. *A. J. Iran. Chem. Soc.* **2014**, *11*, 441. [[CrossRef](#)]
15. Vikneshvaran, S.; Velmathi, S. Impact of Halide-Substituted Chiral Schiff Bases on Corrosion Behaviour of Carbon Steel in Acidic Environment. *J. Nanosci. Nanotechnol.* **2019**, *19*, 4458. [[CrossRef](#)] [[PubMed](#)]
16. Costamagna, J.; Lillo, E.; Matsuhira, B.; Noseda, D.; Villagrán, M. Ni(II) complexes with Schiff bases derived from amino sugars. *Carbohydr. Res.* **2003**, *338*, 1535. [[CrossRef](#)]
17. Chauhan, D.S.; Mazumder, M.A.J.; Quraishi, M.A.; Ansari, K.R.; Suleiman, R.K. Microwave-assisted synthesis of a new Piperonal-Chitosan Schiff base as a bio-inspired corrosion inhibitor for oil-well acidizing. *Int. J. Biol. Macromol.* **2020**, *158*, 231. [[CrossRef](#)]



18. Canton-Díaz, A.M.; Munoz-Flores, B.M.; Moggio, I.; Arias, E.; Turlakov, G.; Angel-Mosqueda, C.D.; Ramirez-Montes, P.I.; Jimenez-Perez, V.M. Molecular structures, DFT studies and their photophysical properties in solution and solid state. Microwave-assisted multicomponent synthesis of organotin bearing Schiff bases. *Mol. Struct.* **2019**, *1180*, 642–650.
19. Antony, R.; Arun, T.; Manickam, S.T. A review on applications of chitosan-based Schiff bases. *Int. J. Biol. Macromol.* **2019**, *129*, 615. [[CrossRef](#)]
20. Wolff, S.K.; Grimwood, D.J.; McKinnon, J.J.; Jayatilaka, D.; Spackman, M.A. *Crystal Explorer 2.1*; University of Western Australia: Perth, Australia, 2007.
21. Frisch, M.J.; Trucks, G.W.; Schlegel, H.B.; Scuseria, G.E.; Robb, M.A.; Cheeseman, J.R.; Scalmani, G.; Barone, V.; Petersson, G.A.; Nakatsuji, H.; et al. *Gaussian 09*; Gaussian Inc.: Wallingford, CT, USA, 2009.
22. O'Boyle, N.M.; Tenderholt, A.L.; Langner, K.M. A Library for Package-Independent Computational Chemistry Algorithms. *J. Comp. Chem.* **2008**, *29*, 839–845. [[CrossRef](#)] [[PubMed](#)]
23. Dennington, R.; Keith, T.A.; Millam, J.M. *GaussView Version*; Semichem Inc.: Shawnee Mission, KS, USA, 2009; Volume 5.
24. Petricek, V.; Dusek, M.; Palatinus, L.; Kristallogr, Z. Crystallographic Computing System JANA2006: General features. *Zeitschrift für Kristallographie-Crystalline Materials* **2014**, *229*, 345–352.
25. Bruker, APEX2, SAINT-Plus, XPREP and SADABS; Bruker AXS Inc.: Madison, WI, USA, 2004.
26. Evans, G.G.; Boeyens, J.A. The linear space of ring conformations. *Acta Cryst.* **1989**, *45*, 581–590. [[CrossRef](#)]
27. Cremer, D.; Pople, J.A. General Definition of ring puckering coordinates. *J. Am. Chem. Soc.* **1975**, *97*, 1354. [[CrossRef](#)]
28. Spackman, M.A.; Jayatilaka, D. Hirshfeld surface analysis. *CrystEngComm* **2009**, *11*, 19. [[CrossRef](#)]
29. Sheldrick, G. *SHELXL-97*; Universität Göttingen: Göttingen, Germany, 1999.
30. Tabti, S.; Djedouani, A.; Aggoun, D.; Warad, I.; Rahmouni, S.; Romdhane, S.; Fouzi, H. Crystal interactions, computational, spectral and thermal analysis of (E)-N'-(thiophen-2-ylmethylene)isonicotinohydrazide as O-N-S-tridentate schiff base ligand. *J. Mol. Struct.* **2018**, *1155*, 11. [[CrossRef](#)]
31. Warad, I.; Abdoh, M.; al Ali, A.; Shivalingegowda, N.; Kumara, K.; Zarrouk, A.; Lokanath, N.K. Synthesis, spectra and X-ray crystallography of dipyrindin-2-ylmethanone oxime and its CuX<sub>2</sub>(oxime)<sub>2</sub> complexes: Thermal, Hirshfeld surface and DFT analysis. *J. Mol. Struct.* **2018**, *1154*, 619–625. [[CrossRef](#)]
32. Warad, I.; Awwadi, F.F.; Al-Ghani, B.A.; Sawafta, A.; Shivalingegowda, N.; Lokanath, N.K.; Mubarak, M.S.; Hadda, T.B.; Zarrouk, A.; Al-Rimawi, F.; et al. Barghouthi, Ultrasound-assisted synthesis of two novel [CuBr(diamine)<sub>2</sub>·H<sub>2</sub>O]Br complexes: Solvatochromism, crystal structure, physicochemical, Hirshfeld surface thermal, DNA/binding, antitumor and antibacterial activities. *S.A. Ultrason. Sonochem.* **2018**, *48*, 1. [[CrossRef](#)] [[PubMed](#)]
33. Aouad, M.R.; Messali, M.; Rezki, N.; Al-Zaqri, N.; Warad, I. Single proton intramigration in novel 4-phenyl-3-((4-phenyl-1H-1,2,3-triazol-1-yl)methyl)-1H-1,2,4-triazole-5(4H)-thione: XRD-crystal interactions, physicochemical, thermal, Hirshfeld surface, DFT realization of thiol/thione tautomerism. *J. Mol. Liq.* **2018**, *264*, 621. [[CrossRef](#)]
34. Aouad, M.R.; Messali, M.; Rezki, N.; Said, M.A.; Lentz, D.; Zubaydi, L.; Warad, I. Synthesis and XRD of neutral NiL complex using unsymmetrical ONNO tetradentate schiff base: Hirshfeld, spectral, DFT and thermal analysis. *J. Mol. Struct.* **2019**, *1180*, 455. [[CrossRef](#)]
35. Hijji, Y.; Benjamin, E.; Butcher, R.; Zarrouk, A.; Warad, I. Crystal structure, spectral, thermal and experimental/computational investigation of Anthracen-benzo [d] thiazol-2-amine new Schiff base derivative. *J. Mol. Struct.* **2021**, *1229*, 129824. [[CrossRef](#)]